Jinde, Y. I.N.; Jiarong, L. I.; Chen, Hao; Wang, Jintao; Peiguang, Y. A.N.; Mengli, L. I.U.; Wenjun, L. I.U.; Wei, L. U.; Zihan, X. U.; Zhang, Wenfei; Wang, Jinzhang; Zhipei, S. U.N.; Ruan, Shuangchen

Large-area highly crystalline WSe2 atomic layers for ultrafast pulsed lasers

Published in:
Optics Express

DOI:
10.1364/OE.25.030020

Published: 27/11/2017

Document Version
Publisher's PDF, also known as Version of record

Please cite the original version:
Jinde, Y. I. N., Jiarong, L. I., Chen, H., Wang, J., Peiguang, Y. A. N., Mengli, L. I. U., Wenjun, L. I. U., Wei, L. U., Zihan, X. U., Zhang, W., Wang, J., Zhipei, S. U. N., & Ruan, S. (2017). Large-area highly crystalline WSe_2 atomic layers for ultrafast pulsed lasers. *Optics Express*, *25*(24), 30020-30031. https://doi.org/10.1364/OE.25.030020

Research Article | Vol. 25, No. 24 | 27 Nov 2017 | OPTICS EXPRESS 30020
Optics EXPRESS

Large-area highly crystalline WSe_2 atomic layers for ultrafast pulsed lasers

JINDE YIN,[1,2,7] JIARONG LI,[1,7] HAO CHEN,[1] JINTAO WANG,[1,2] PEIGUANG YAN[1,8] MENGLI LIU,[3] WENJUN LIU,[3,9] WEI LU,[4] ZIHAN XU,[5] WENFEI ZHANG,[1] JINZHANG WANG,[1] ZHIPEI SUN,[6] AND SHUANGCHEN RUAN[1]

[1]*Shenzhen Key Laboratory of Laser Engineering, College of Optoelectronic Engineering, Shenzhen University, Shenzhen 518060, China*
[2]*Key Laboratory of Optoelectronic Devices and Systems of Ministry of Education and Guangdong Province, College of Optoelectronic Engineering, Shenzhen University, Shenzhen 518060, China*
[3]*State Key Laboratory of Information Photonics and Optical Communications, School of Science, P. O. Box 91, Beijing University of Posts and Telecommunications, Beijing 100876, China*
[4]*University Research Facility in Materials Characterization and Device Fabrication, Hong Kong Polytechnic University, Hong Kong, China*
[5]*6Carbon Technology (Shenzhen), Shenzhen 518000, China*
[6]*Department of Electronics and Nanoengineering, Aalto University, Tietotie 3, FI-00076 Espoo, Finland*
[7]*These authors contributed equally to this work.*
[8]*yanpg@szu.edu.cn*
[9]*jungliu@bupt.edu.cn*

Abstract: Large-area and highly crystalline transition metal dichalcogenides (TMDs) films possess superior saturable absorption compared to the TMDs nanosheet counterparts, which make them more suitable as excellent saturable absorbers (SA) for ultrafast laser technology. Thus far, the nonlinear optical properties of large-scale WSe_2 and its applications in ultrafast photonics have not yet been fully investigated. In this work, the saturable absorption of chemical vapor deposition (CVD) grown WSe_2 films with large-scale and high quality are studied and the use of WSe_2 films as a broadband SA for passively mode-locked fiber lasers at both 1.5 and 2 μm ranges is demonstrated. To enhance the light-material interaction, large-area WSe_2 film is tightly transferred onto the side wall of a microfiber to form a hybrid structure, which realizes strong evanescent wave interaction between light and WSe_2 film. The integrated microfiber-WSe_2 device shows a large modulation depth of 54.5%. Using the large-area WSe_2 as a mode-locker, stable soliton mode-locked pulse generation is achieved and the pulse durations of 477 fs (at 1.5 μm) and 1.18 ps (at 2.0 μm) are demonstrated, which suggests that the large-area and highly crystalline WSe_2 films afford an excellent broadband SA for ultrafast photonic applications.

OCIS codes: (160.4330) Nonlinear optical materials; (060.3510) Lasers, fiber; (140.4050) Mode-locked lasers.

References and links

1. Q. H. Wang, K. Kalantar-Zadeh, A. Kis, J. N. Coleman, and M. S. Strano, "Electronics and optoelectronics of two-dimensional transition metal dichalcogenides," Nat. Nanotechnol. **7**(11), 699–712 (2012).
2. K. F. Mak and J. Shan, "Photonics and optoelectronics of 2D semiconductor transition metal dichalcogenides," Nat. Photonics **10**, 216–226 (2016).
3. R. Lv, J. A. Robinson, R. E. Schaak, D. Sun, Y. Sun, T. E. Mallouk, and M. Terrones, "Transition metal dichalcogenides and beyond: synthesis, properties, and applications of single- and few-layer nanosheets," Acc. Chem. Res. **48**(1), 56–64 (2015).
4. Z. Sun, A. Martinez, and F. Wang, "Optical modulators with 2D layered materials," Nat. Photonics **10**, 227–238 (2016).
5. Y. Zhang, T. R. Chang, B. Zhou, Y. T. Cui, H. Yan, Z. Liu, F. Schmitt, J. Lee, R. Moore, Y. Chen, H. Lin, H. T. Jeng, S. K. Mo, Z. Hussain, A. Bansil, and Z. X. Shen, "Direct observation of the transition from indirect to direct bandgap in atomically thin epitaxial $MoSe_2$," Nat. Nanotechnol. **9**(2), 111–115 (2014).

#308198 https://doi.org/10.1364/OE.25.030020
Journal © 2017 Received 29 Sep 2017; revised 9 Nov 2017; accepted 9 Nov 2017; published 16 Nov 2017

Optics EXPRESS

6. W. Zhao, R. M. Ribeiro, M. Toh, A. Carvalho, C. Kloc, A. H. Castro Neto, and G. Eda, "Origin of indirect optical transitions in few-layer MoS_2, WS_2, and WSe_2," Nano Lett. **13**(11), 5627–5634 (2013).
7. W. Zhao, Z. Ghorannevis, L. Chu, M. Toh, C. Kloc, P. H. Tan, and G. Eda, "Evolution of electronic structure in atomically thin sheets of WS_2 and WSe_2," ACS Nano **7**(1), 791–797 (2013).
8. B. Radisavljevic, A. Radenovic, J. Brivio, V. Giacometti, and A. Kis, "Single-layer MoS_2 transistors," Nat. Nanotechnol. **6**(3), 147–150 (2011).
9. H. Schmidt, S. Wang, L. Chu, M. Toh, R. Kumar, W. Zhao, A. H. C. Neto, J. Martin, S. Adam, B. Özyilmaz, and G. Eda, "Transport properties of monolayer MoS_2 grown by chemical vapor deposition," Nano Lett. **14**(4), 1909–1913 (2014).
10. J. S. Rhyee, J. Kwon, P. Dak, J. H. Kim, S. M. Kim, J. Park, Y. K. Hong, W. G. Song, I. Omkaram, M. A. Alam, and S. Kim, "High-mobility transistors based on large-area and highly crystalline CVD-grown $MoSe_2$ films on insulating substrates," Adv. Mater. **28**(12), 2316–2321 (2016).
11. S. Wang, H. Yu, H. Zhang, A. Wang, M. Zhao, Y. Chen, L. Mei, and J. Wang, "Broadband few-layer MoS_2 saturable absorbers," Adv. Mater. **26**(21), 3538–3544 (2014).
12. D. Mao, B. Du, D. Yang, S. Zhang, Y. Wang, W. Zhang, X. She, H. Cheng, H. Zeng, and J. Zhao, "Nonlinear saturable absorption of liquid-exfoliated molybdenum/tungsten ditelluride nanosheets," Small **12**(11), 1489–1497 (2016).
13. J. Koo, Y. I. Jhon, J. Park, J. Lee, and Y. M. Jhon, "Near-infrared saturable absorption of defective bulk-structured WTe2 for femtosecond laser mode-locking," Adv. Funct. Mater. **26**, 7454–7461 (2016).
14. P. Yan, H. Chen, J. Yin, Z. Xu, J. Li, Z. Jiang, W. Zhang, J. Wang, I. L. Li, Z. Sun, and S. Ruan, "Large-area tungsten disulfide for ultrafast photonics," Nanoscale **9**(5), 1871–1877 (2017).
15. H. Chen, J. Yin, J. Yang, X. Zhang, M. Liu, Z. Jiang, J. Wang, Z. Sun, T. Guo, W. Liu, and P. Yan, "Transition-metal dichalcogenides heterostructure saturable absorbers for ultrafast photonics," Opt. Lett. **42**(21), 4279–4282 (2017).
16. M. Zhang, G. Hu, G. Hu, R. C. T. Howe, L. Chen, Z. Zheng, and T. Hasan, "Yb- and Er-doped fiber laser Q-switched with an optically uniform, broadband WS_2 saturable absorber," Sci. Rep. **5**, 17482 (2015).
17. H. Chen, Y. Chen, J. Yin, X. Zhang, T. Guo, and P. Yan, "High-damage-resistant tungsten disulfide saturable absorber mirror for passively Q-switched fiber laser," Opt. Express **24**(15), 16287–16296 (2016).
18. H. Li, J. Wu, Z. Yin, and H. Zhang, "Preparation and applications of mechanically exfoliated single-layer and multilayer MoS_2 and WSe_2 nanosheets," Acc. Chem. Res. **47**(4), 1067–1075 (2014).
19. H. Zhou, C. Wang, J. C. Shaw, R. Cheng, Y. Chen, X. Huang, Y. Liu, N. O. Weiss, Z. Lin, Y. Huang, and X. Duan, "Large area growth and electrical properties of p-type WSe_2 atomic layers," Nano Lett. **15**(1), 709–713 (2015).
20. H. J. Chuang, X. Tan, N. J. Ghimire, M. M. Perera, B. Chamlagain, M. M. C. Cheng, J. Yan, D. Mandrus, D. Tománek, and Z. Zhou, "High mobility WSe_2 p- and n-type field-effect transistors contacted by highly doped graphene for low-resistance contacts," Nano Lett. **14**(6), 3594–3601 (2014).
21. B. W. H. Baugher, H. O. H. Churchill, Y. Yang, and P. Jarillo-Herrero, "Optoelectronic devices based on electrically tunable p-n diodes in a monolayer dichalcogenide," Nat. Nanotechnol. **9**(4), 262–267 (2014).
22. J. S. Ross, P. Klement, A. M. Jones, N. J. Ghimire, J. Yan, D. G. Mandrus, T. Taniguchi, K. Watanabe, K. Kitamura, W. Yao, D. H. Cobden, and X. Xu, "Electrically tunable excitonic light-emitting diodes based on monolayer WSe_2 p-n junctions," Nat. Nanotechnol. **9**(4), 268–272 (2014).
23. B. Chen, X. Zhang, K. Wu, H. Wang, J. Wang, and J. Chen, "Q-switched fiber laser based on transition metal dichalcogenides MoS_2, $MoSe_2$, WS_2, and WSe_2," Opt. Express **23**(20), 26723–26737 (2015).
24. D. Mao, X. She, B. Du, D. Yang, W. Zhang, K. Song, X. Cui, B. Jiang, T. Peng, and J. Zhao, "Erbium-doped fiber laser passively mode locked with few-layer WSe_2/$MoSe_2$ nanosheets," Sci. Rep. **6**, 23583 (2016).
25. R. Wei, H. Zhang, X. Tian, T. Qiao, Z. Hu, Z. Chen, X. He, Y. Yu, and J. Qiu, "MoS_2 nanoflowers as high performance saturable absorbers for an all-fiber passively Q-switched erbium-doped fiber laser," Nanoscale **8**(14), 7704–7710 (2016).
26. H. Xia, H. Li, C. Lan, C. Li, X. Zhang, S. Zhang, and Y. Liu, "Ultrafast erbium-doped fiber laser mode-locked by a CVD-grown molybdenum disulfide (MoS_2) saturable absorber," Opt. Express **22**(14), 17341–17348 (2014).
27. J. K. Huang, J. Pu, C. L. Hsu, M. H. Chiu, Z. Y. Juang, Y. H. Chang, W. H. Chang, Y. Iwasa, T. Takenobu, and L. J. Li, "Large-area synthesis of highly crystalline WSe_2 monolayers and device applications," ACS Nano **8**(1), 923–930 (2014).
28. J. Huang, L. Yang, D. Liu, J. Chen, Q. Fu, Y. Xiong, F. Lin, and B. Xiang, "Large-area synthesis of monolayer WSe_2 on a SiO_2/Si substrate and its device applications," Nanoscale **7**(9), 4193–4198 (2015).
29. X. Lu, M. I. B. Utama, J. Lin, X. Gong, J. Zhang, Y. Zhao, S. T. Pantelides, J. Wang, Z. Dong, Z. Liu, W. Zhou, and Q. Xiong, "Large-area synthesis of monolayer and few-layer $MoSe_2$ films on SiO_2 substrates," Nano Lett. **14**(5), 2419–2425 (2014).
30. J. Chen, B. Liu, Y. Liu, W. Tang, C. T. Nai, L. Li, J. Zheng, L. Gao, Y. Zheng, H. S. Shin, H. Y. Jeong, and K. P. Loh, "Chemical vapor deposition of large-sized hexagonal WSe_2 crystals on dielectric substrates," Adv. Mater. **27**(42), 6722–6727 (2015).
31. H. Li, G. Lu, Y. Wang, Z. Yin, C. Cong, Q. He, L. Wang, F. Ding, T. Yu, and H. Zhang, "Mechanical exfoliation and characterization of single- and Few-Layer Nanosheets of WSe_2, TaS_2, and $TaSe_2$," Small **9**(11), 1974–1981 (2013).

32. D. Kozawa, R. Kumar, A. Carvalho, K. Kumar Amara, W. Zhao, S. Wang, M. Toh, R. M. Ribeiro, A. H. Castro Neto, K. Matsuda, and G. Eda, "Photocarrier relaxation pathway in two-dimensional semiconducting transition metal dichalcogenides," Nat. Commun. **5**, 4543 (2014).
33. J. Ma, G. Q. Xie, P. Lv, W. L. Gao, P. Yuan, L. J. Qian, H. H. Yu, H. J. Zhang, J. Y. Wang, and D. Y. Tang, "Graphene mode-locked femtosecond laser at 2 μm wavelength," Opt. Lett. **37**(11), 2085–2087 (2012).
34. J. Sotor, G. Sobon, M. Kowalczyk, W. Macherzynski, P. Paletko, and K. M. Abramski, "Ultrafast thulium-doped fiber laser mode locked with black phosphorus," Opt. Lett. **40**(16), 3885–3888 (2015).
35. M. Jung, J. Lee, J. Park, J. Koo, Y. M. Jhon, and J. H. Lee, "Mode-locked, 1.94-μm, all-fiberized laser using WS_2 based evanescent field interaction," Opt. Express **23**(15), 19996–20006 (2015).
36. J. Lee, J. Koo, J. Lee, Y. M. Jhon, and J. H. Lee, "All-fiberized, femtosecond laser at 1912 nm using a bulk-like $MoSe_2$ saturable absorber," Opt. Mater. Express **7**(8), 2968–2979 (2017).
37. R. I. Woodward, E. J. R. Kelleher, R. C. T. Howe, G. Hu, F. Torrisi, T. Hasan, S. V. Popov, and J. R. Taylor, "Tunable Q-switched fiber laser based on saturable edge-state absorption in few-layer molybdenum disulfide (MoS_2)," Opt. Express **22**(25), 31113–31122 (2014).
38. M. Trushin, E. J. R. Kelleher, and T. Hasan, "Theory of edge-state optical absorption in two-dimensional transition metal dichalcogenide flakes," Phys. Rev. B **94**, 155301 (2016).
39. J. Wang, X. Liang, G. Hu, Z. Zheng, S. Lin, D. Ouyang, X. Wu, P. Yan, S. Ruan, Z. Sun, and T. Hasan, "152 fs nanotube-mode-locked thulium-doped all-fiber laser," Sci. Rep. **6**, 28885 (2016).
40. Q. Bao, H. Zhang, Y. Wang, Z. Ni, Y. Yan, Z. X. Shen, K. P. Loh, and D. Y. Tang, "Atomic-layer graphene as a saturable absorber for ultrafast pulsed lasers," Adv. Funct. Mater. **19**, 3077–3083 (2009).
41. Z. Sun, T. Hasan, F. Torrisi, D. Popa, G. Privitera, F. Wang, F. Bonaccorso, D. M. Basko, and A. C. Ferrari, "Graphene mode-locked ultrafast laser," ACS Nano **4**(2), 803–810 (2010).
42. H. Mu, S. Lin, Z. Wang, S. Xiao, P. Li, Y. Chen, H. Zhang, H. Bao, S. P. Lau, C. Pan, D. Fan, and Q. Bao, "Black phosphorus–polymer composites for pulsed lasers," Adv. Opt. Mater. **3**, 1447–1453 (2015).
43. D. Li, H. Jussila, L. Karvonen, G. Ye, H. Lipsanen, X. Chen, and Z. Sun, "Polarization and thickness dependent absorption properties of black phosphorus: new saturable absorber for ultrafast pulse generation," Sci. Rep. **5**, 15899 (2015).
44. J. Li, H. Luo, B. Zhai, R. Lu, Z. Guo, H. Zhang, and Y. Liu, "Black phosphorus: a two-dimension saturable absorption material for mid-infrared Q-switched and mode-locked fiber lasers," Sci. Rep. **6**, 30361 (2016).
45. G. Hu, T. Albrow-Owen, X. Jin, A. Ali, Y. Hu, R. C. T. Howe, K. Shehzad, Z. Yang, X. Zhu, R. I. Woodward, T. C. Wu, H. Jussila, J. B. Wu, P. Peng, P. H. Tan, Z. Sun, E. J. R. Kelleher, M. Zhang, Y. Xu, and T. Hasan, "Black phosphorus ink formulation for inkjet printing of optoelectronics and photonics," Nat. Commun. **8**(1), 278 (2017).

1. Introduction

Two-dimensional (2D) layered transition metal dichalcogenides (TMDs) have attracted worldwide attentions due to their unique electronic and photonic properties [1–4]. Recent reports have demonstrated that the energy band structures of the semiconducting TMDs show a unique transition from indirect to direct band gap as the thickness is reduced to monolayer [5–7]. These monolayer TMDs with direct band gap can offer exciting opportunities for potential applications in both electronic and optoelectronic devices [4,8–17]. Among all TMD materials, WSe_2 has recently received huge interest due to their distinctive electro-optical properties and remarkable electronic characteristics [18–24]. For example, it has been recently reported that mechanically exfoliated monolayer WSe_2 was adopted to fabricate high performance n-type and p-type field-effect transistors [18–20]. Monolayer WSe_2 p-n junctions and heterostructure p-n junctions composed of p-type WSe_2 and n-type other TMDs (WSe_2, MoS_2, or WS_2) were demonstrated for optoelectronic devices [21,22]. Meanwhile, for the ultrafast photonic applications, it has also been recently reported that liquid-phase exfoliation method prepared WSe_2 nanosheets were employed as saturable absorbers (SAs) for passively Q-switched and mode-locked pulse generation due to their excellent nonlinear optical absorption and ultrafast carrier dynamics [23,24]. However, the lateral size and thickness of WSe_2 nanosheets fabricated by both mechanical exfoliation and liquid-phase exfoliation are limited in a few to a few tens of micrometers. As the outstanding optical properties are closely related to the size and morphology of the materials [25], the uncontrollable and non-uniform WSe_2 nanosheets usually result in a low surface-to-volume ratio and then renovate their properties. Compared to the TMDs nanosheets, one can expect that large-area TMDs films can possess better optical properties. For example, recent demonstrations have indicated that the chemical vapor deposition (CVD) grown large-area MoS_2 films have shown remakable modulation depth of 35.4% [26], which is over one order of magnitude larger than

Optics EXPRESS

that of the MoS_2 nanosheets [23]. Unlike MoS_2, large-area atomic-layered WSe_2 for optoelectronic devices yet remains a significant challenge as the chemical reactivity of selenium is much lower than that of sulfur. The CVD method has been recently presented for synthesis of large-scale WSe_2 films by introducing hydrogen as a strong reducer during the synthesis reaction [19,27,28]. The excellent electronic characteristics of large-area WSe_2 films such as mobility of 350 $cm^2v^{-1}s^{-1}$ and on/off ratio of 10^8 have been studied in electronic devices [19], while their nonlinear optical properties and the potential applications in ultrafast photonics have remained elusive.

Large-area atomically thin WSe_2 films integrated with microfiber structures can offer tight optical confinement for enhancing the light-material interaction, and further provide an ideal platform for studying their nonlinear optical properties and their applications with superior mode-locking performance. In this contribution, large-area atomically thin WSe_2 film was grown on a sapphire substrate by a CVD method. The material characterization confirmed the high quality of the as-grown WSe_2 film. The large-area WSe_2 shows remarkable nonlinear optical performance, such as a large modulation depth (~54.5%) and low saturable intensity (2.97 $MW \cdot cm^{-2}$). Based on the microfiber WSe_2 SA with strong evanescent wave coupling effect, a stable soliton mode-locked erbium-doped fiber (EDF) laser was obtained with pulse duration of 477 fs, which is the shortest mode-locked laser based on WSe_2 SAs. Moreover, we also demonstrated the mode-locked thulium-doped fiber (TDF) laser based on WSe_2 SA at 2 μm regime.

2. Growth and characterization of WSe_2 atomic layers

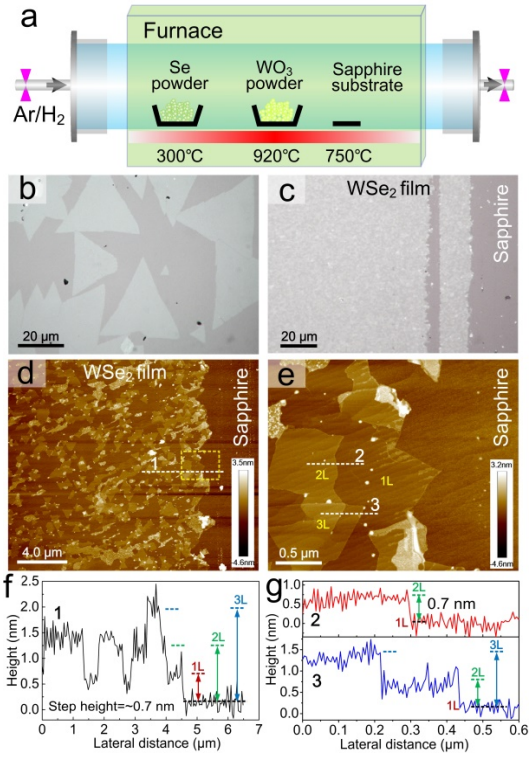

Fig. 1. CVD-growth of large-area WSe_2 continuous film on a sapphire substrate. (a) Schematic of experimental setup for CVD growth of WSe_2 atomic layers. (b) Optical microscope (OM) image of the monolayer WSe_2 triangles grown at 790 °C. (c) OM image of the few-layer WSe_2 continuous film grown at 750 °C. (d) AFM image of the WSe_2 film close to film edge. (e) Magnified AFM image at the dashed lines area in (d). (f, g) Height profiles of line scan across the WSe_2 layers corresponding to along the lines 1, 2, and 3 in (d), and (e), respectively.

Optics EXPRESS

Large-area and highly crystalline WSe_2 film was grown on a sapphire substrate by using a CVD method, and the experimental setup was illustrated in Fig. 1(a). The growth processes were performed in a quartz tube furnace using WO_3 and Selenium (Se) powders as starting materials. The WO_3 powders (~0.1g) were placed in a ceramic boat located in the heating zone center. The Se powders (~0.5 g) in a separate ceramic boat were placed at a distance ~50 cm at the upper stream of WO_3 powders. The sapphire substrates were put at the downstream side at ~20 cm away from the heating zone center. During the reaction, the Se and WO_3 vapors were brought on the targeting sapphire substrates by Ar/H_2 flow gas (Ar = 100 sccm, H_2 = 10 sccm, chamber pressure = 1 Torr). The temperature distribution along quartz tube is approximatively Gaussian. The growth temperature is an important factor, which directly determines the morphology of WSe_2. The optical microscope (OM) image in Fig. 1(b) shows the monolayer WSe_2 triangles grown at substrate temperature of 790 °C, and the lateral size of triangle is typically larger than 10 μm with a maximum size up to 50 μm. With further growth, additional layers were grown on the top of WSe_2 triangles, instead of a continuous monolayer film. Such additional layer growth result at high temperature during CVD synthesis is consistent with previous reports [19]. The lateral size of triangles might be limited by the lattice mismatch between WSe_2 and sapphire substrates. In our experiment, we expected the WSe_2 triangles merge together to form a large-area continuous film for ultrafast photonic applications with superior performance. As we decrease the substrate temperature to 750 °C, the small WSe_2 domains merge to form a continuous film on sapphire substrate, since a lower growth temperature typically results in a higher nucleation density [27]. The continuous film with large-scale can be clearly seen in Fig. 1(c) due to the high contrast of color display between WSe_2 layers and sapphire substrate. The morphology and height profile of WSe_2 film are investigated by using atomic force microscope (AFM, Bruker Dimension Icon). The AFM image in Fig. 1(d) shows the morphology of few-layer WSe_2. We observe the CVD grown monolayer, bilayer and few-layer small domains on the top of continuous monolayer. The height profile in Fig. 1(f) shows the thickness of the as-grown film along the line 1 in Fig. 1(d), proving the layer-by-layer structure of the film. The thickness of monolayer is around 0.7 nm, which is in a good agreement with the exfoliated monolayer WSe_2 [19]. The magnified AFM image in Fig. 1(e) for the area squared by dashed lines in Fig. 1(d) reveals the monolayer (1L), bilayer (2L) and trilayer (3L) of the as-grown film. The AFM cross-sectional height profiles at lines 2 and 3 in Fig. 1(e) further confirms the layers numbers according to the step height of ~0.7 nm, as shown in Fig. 1(g). The additional WSe_2 triangles with different layers bonded on the top of the monolayer WSe_2 continuous film, which can strengthen the mechanical strength of the WSe_2 film for the benefit of further large-scale transfer process.

The crystal structure of WSe_2 film was probed by a transmission electron microscopy (TEM, JEM-2010) operated at an electron accelerating voltage of 200 kV. The WSe_2 samples were transferred onto a carbon grid using polymethyl methacrylate (PMMA) transfer technique [29]. Low magnification TEM image in Fig. 2(a) shows the film-like structure of the transferred WSe_2 sample. From Fig. 2(b), the high-resolution TEM (HRTEM) image at the cross area in Fig. 2(a) shows the periodic atom arrangement of the WSe_2 atomic layer, demonstrating that the CVD-grown WSe_2 film is highly crystalline. The inset shows the selected area electron diffraction (SAED) pattern with clear six-fold symmetry diffraction spots, revealing the hexagonal lattice of WSe_2 film. Figure 2(c) shows the magnified HRTEM image for the area squared by dashed lines in Fig. 2(b), and the lattice constant was measured to be around 0.33nm, consistent with that of previously reported WSe_2 [27]. The characteristic peaks of energy dispersive spectroscopy (EDS) spectrum in Fig. 2(d) are in a good agreement with the previously reported results [19,30]. The presence of Cu is probably induced from the carbon grid. The EDS spectrum reveals that the atomic ratio between W and Se is about 1:2.1, which suggest tungsten defects in the WSe_2 film. Figure 2(e) shows the Raman spectra of hexagonal WSe_2 with different thickness, which were collected on a Raman

Optics EXPRESS

system (HORIBA LabRAM HR800) using a laser excitation of 532nm. All WSe_2 layers reveal two characteristic peaks located at 252 cm^{-1} and 262 cm^{-1}, which are assignable to the in-plane E_{2g}^1 mode and out-of-plane A_{1g} mode (insert of Fig. 2(e)), respectively [28,31]. Note that the Raman peak B_{2g}^1 mode at 309 cm^{-1} is attributed to the interlayer interactions [31]. The B_{2g}^1 mode is absent in 1L WSe_2, which further confirms the monolayer film. The B_{2g}^1 mode is active in 2L and few-layer WSe_2 film reflecting the presence of the interlayer interaction [18,19]. The strong Raman peaks suggest the high quality of WSe_2 film grown by CVD method.

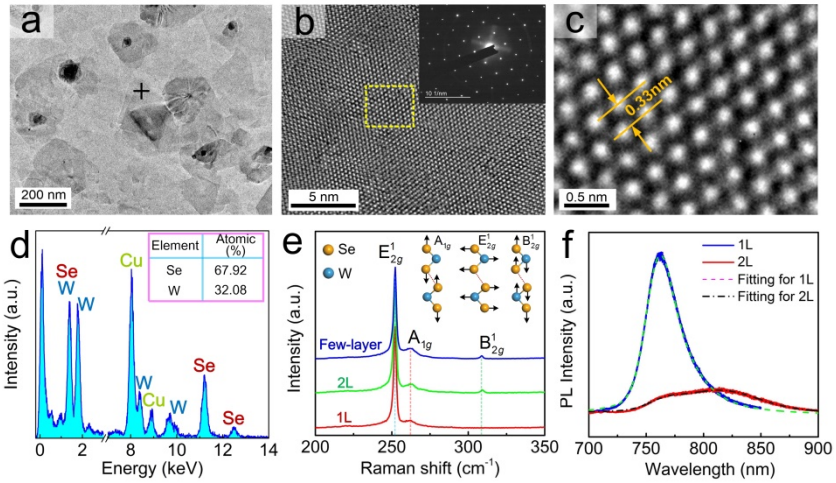

Fig. 2. Characterization of the CVD-grown WSe_2 Film. (a) Low-magnification TEM image of WSe_2 film transferred onto a carbon grid. (b) HRTEM image of WSe_2 with periodic atom arrangement, the inset shows its SAED pattern with six-fold symmetry diffraction spots. (c) Magnified HRTEM image for the marked area in (b). (d) The measured EDS spectrum with the energy range of 0~14 keV. (e) Raman spectra of the monolayer, bilayer, and few-layer WSe_2 film, the inset shows the atomic displacement of three Raman-active modes (A_{1g}, E_{2g}^1, and B_{2g}^1) in WSe_2. (f) PL spectra of monolayer and bilayer WSe_2, all Raman spectra and PL spectra are excited by a 532 nm laser.

The optical properties of WSe_2 film were further investigated using photoluminescence (PL). Figure 2(f) shows that the monolayer WSe_2 film exhibits strong emission at approximately 762 nm (1.63 eV) arising from direct gap transitions at K point, in a good agreement with previous reports [19,27,32]. From bilayer PL spectrum, the emission intensity is dramatically reduced. We can observe two PL peaks attributed to direct and indirect band gap emission at $K \rightarrow K$ and $K \rightarrow \Gamma$ points, respectively [6,7]. Both emission spectra were fitted with Gaussian peaks located at 766 nm (1.62eV) and 812 nm (1.53eV). The layer-dependent PL spectra confirm the transition from direct to indirect bandgap with the increasing of thickness. Note that the absence of indirect gap emission peak in the PL spectrum of 1L WSe_2 further suggests that the monolayer WSe_2 film has direct band gap. The PL spectra suggest the unique bandgap structure and excellent optical properties of the as-grown WSe_2 film.

3. Nonlinear optical properties

We transferred the WSe_2 films onto microfibers to fabricate WSe_2-based fiber SAs. Different from the previous WSe_2-polymer composite [23,24], the microfiber WSe_2 SA cannot only enhance the nonlinear optical absorption through the strong evanescent wave interaction within a long fused waist zone, but also increase the capability to thermal damage resistance and compatibility to fiber components. Herein, we employed a polymethyl methacrylate (PMMA) assisted method to transfer the WSe_2 film from sapphire substrate onto the waist of

microfiber. Figure 3(a) schematically shows the preparation process of the SAs fabrication. A thin PMMA film was firstly spin coated on the upper surface of WSe_2 film. The WSe_2-PMMA composite was then stripped from the sapphire substrate after drying up. The PMMA in composite was etched off by acetone to obtain pure WSe_2 film. After that, the pure WSe_2 film was moved to deionized (DI) water. Due to the strong surface tension of water, the WSe_2 would float on the top surface of the DI water smoothly. Note that the DI water is used as not only the residues cleaning fluid, but also the supporting medium of WSe_2 film. A pieces of WSe_2 film with the size of ~2 × 4mm can be observed on water in Fig. 3(a). The free-standing WSe_2 film was finally transferred onto the waist of microfiber by bailing process with the micromechanical control under a microscope. The microfiber is fabricated by fiber-tapering equipment with single mode fiber (SMF-28e). The waist diameter of the microfiber is around 11 μm and the length of WSe_2 covered section is about 2 mm. After the residual DI water on WSe_2 volatilized at room temperature, the WSe_2 film tightly attached on the side wall of the microfiber by Van der Waals force, as shown in the scanning electron microscopy (SEM, HITACHI SU8000) image in Fig. 3(b). The magnified SEM image in Fig. 3(c) reveals large-area WSe_2 film integrated with microfiber closely and smoothly. The few wrinkles on WSe_2 film visually confirm that WSe_2 film was successfully transferred onto the waist of microfiber. The OM image in Fig. 3(d) shows the transferred WSe_2 film near edge area. The WSe_2 film can be clearly seen according to the metallic reflected light. Once a 630 nm laser beam was launched into the microfiber, scattered light from WSe_2 film can be observed in the OM image of Fig. 3(e), which suggests the strong light-WSe_2 interaction through evanescent wave coupling effect.

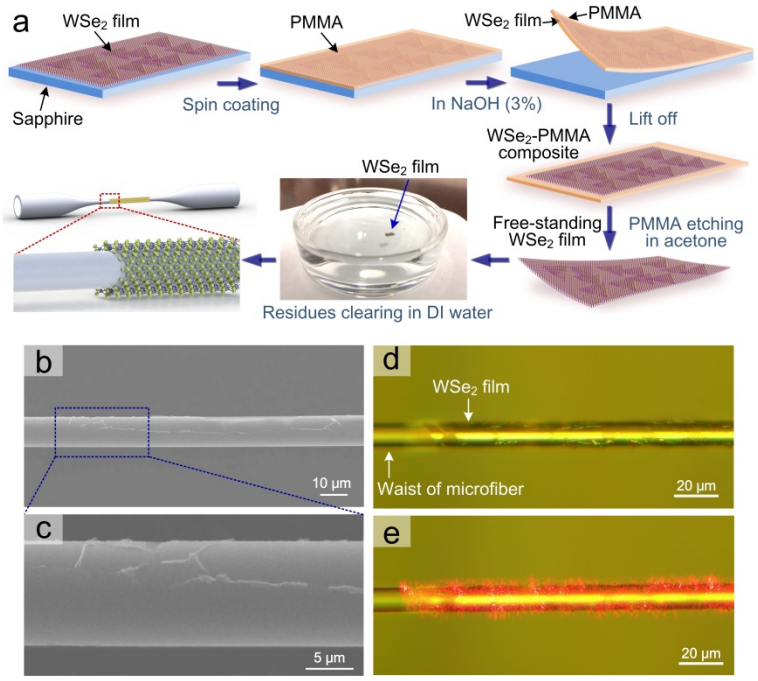

Fig. 3. Fabrication of WSe_2 SA integrated with a microfiber microstructure. (a) Schematic of PMMA-assisted WSe_2 SA fabrication process by transferring the WSe_2 film from the sapphire substrate onto the waist section of the microfiber. (b) SEM image of the microfiber covered with large-area WSe_2 film. (c) Magnified SEM image at the marked area in (b), indicating close integration between WSe_2 film and microfiber. (d, e) OM images of WSe_2 film covered microfiber before and after launching 630 nm laser beam.

The linear absorption of few-layer WSe_2 film from 1 to 2 um was measured by using a UV/VIS/NIR spectrophotometer (Cary 5000). The experimental results are shown in Fig.

Optics EXPRESS

4(a), the absorbance of few-layer WSe_2 film at 1550 and 1990 nm are measured to be 8.22% and 4.87%, respectively. The nonlinear optical absorption of the microfiber WSe_2 SA was studied by a simple two-terminal power-dependent measurement at 1550 nm. The representative result from the microfiber WSe_2 SA is shown in Fig. 4(b). It is found that the transmission is closely related to the pump intensity due to saturable absorption. From Fig. 4(b), we note low saturation intensity of 2.97 $MW \cdot cm^{-2}$ is obtained. The modulation depth is measured to be ~54.5% at 1550 nm, which is one order of magnitude larger than that of previous WSe_2 nanoflakes [23,24]. Moreover, the modulation depth at 1864 nm is measured to be ~1.83% by using the similar method, as shown in Fig. 4(c), which is the same order magnitude as that of graphene, black phosphorus, WS_2 and $MoSe_2$ at that range [33–36]. Note that the modulation depth at 1.9 μm is much smaller than that at 1.5 μm, which is mainly limited by the high transmission loss (~90%) of microfiber at this region. We believe that the relatively large modulation depth of WSe_2 SA is originated from the enhanced light-materials interaction in large-scale WSe_2 film during optical absorption process. Compared to the discrete light-materials interaction in the SAs based on nanosheets, continuous light-materials interaction in a long section (~2mm) of WSe_2 film covered region provides much more photo-generated carriers for band filling, which has contributed significantly to increasing of the modulation depth. The large-area WSe_2 film with promising saturable absorption was expected to achieve stable mode-locking operation with ultrashort pulse duration in all fiber laser system. Surprisingly, it is worth to note that the photon energies (0.8 eV and 0.67 eV) of WSe_2 broadband saturable absorption are lower than the material direct bandgap (1.63 eV). The mechanism of saturable absorption at 0.8 eV and 0.67 eV originates from the sub-bandgap absorption due to the edges or defects in the small triangular shapes of WSe_2, which also has been experimentally and theoretically demonstrated in other TMDs nanoflakes [37,38]. For example, recent reports have demonstrated the broadband saturable absorption of MoS_2 due to the introduction of both Mo and S defects [11,37]. In our work, the W defects of WSe_2 films identified from the EDS spectrum and the edges of small WSe_2 triangles observed from the AFM image may make significant contribution to the broadband saturable absorption, which is analogous to that of previously reported MoS_2 [11,37,38].

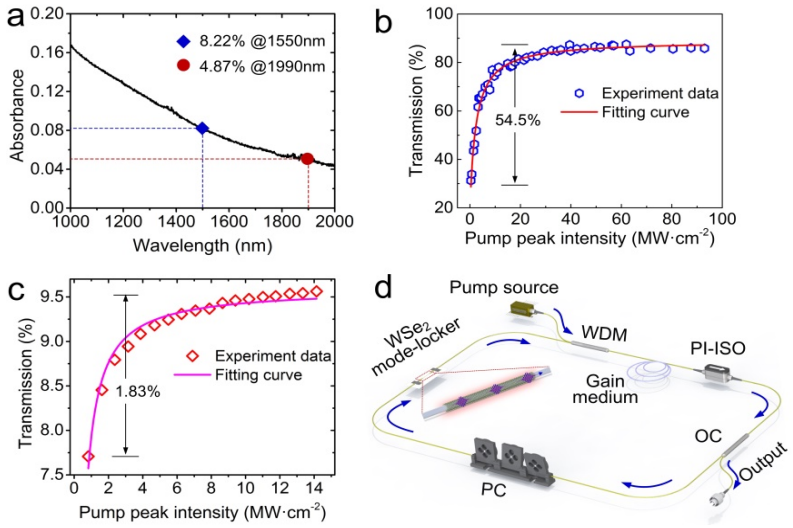

Fig. 4. (a) The linear absorption of few-layer WSe_2 film from 1.0 to 2.0 μm. (b, c) The nonlinear absorption curves of microfiber WSe_2 SA at 1550 nm and 1864 nm. (d) Schematic illustration of the typical ring cavity of the mode-locked fiber laser based on the microfiber WSe_2 SA. WDM: wavelength division multiplexer; PI-ISO: polarization-independent isolator; OC: optical coupler; PC: polarization controller.

Optics EXPRESS

4. Ultrafast fiber laser application

As the microfiber WSe_2 SA was incorporated into the fiber laser cavity, passively mode-locked fiber lasers at 1.5 and 2 μm spectral regions were operated using EDF (Liekki 110-4/125) and TDF (Nufern SM-TSF-9/125) as gain materials, respectively. Figure 4(d) shows the experimental setup of the WSe_2 mode-locked fiber laser. In mode-locked EDF laser cavity, a section of 0.7 m EDF with GVD of 12 $ps^2 \cdot km^{-1}$ as gain medium was pumped by a 976 nm LD through a 980/1550 nm WDM. A PI-ISO at 1550 nm was adopted to ensure the unidirectional laser operation. The cavity polarization state and intra-cavity birefringence were adjusted by a PC. A 20/80 OC was employed as 20% output. The output optical spectrum, pulse duration, and RF spectrum were simultaneously monitored by optical spectrum analyzer (Yokogawa AQ6370C), autocorrelator (APE Pulsecheck) and RF spectrum analyzer (ROHDE & SCHWARZ FSV13) integrated with an InGaAs PIN photodetector (EOT ET-3500FEXT). In this laser ring cavity, no polarization-dependent components were used to avoid self-starting mode-locking operation arising from the nonlinear polarization evolution (NPE). Furthermore, as we change the polarization of input light passing through microfiber-based WSe_2 SA, the polarization dependent loss (PDL) maintains in a small range of 60.72%~62.84% at 1550 nm with 3.21 mW input power, which confirms the PDL could be ignored in the microfiber based WSe_2 SA to avoid undesired NPE effect. Moreover, it is well known that the stable and ultrashort pulse trains can be generated in a passively mode-locked laser after achieving the balance between the self-phase modulation (SPM) and negative group velocity dispersion (GVD) in laser cavity [39]. The WSe_2 SA has normal dispersion, but the accurate value could not be calculated yet because of the hybrid structure of microfiber and WSe_2 film. In order to achieve stable soliton mode-locking operation, we tried to add extra SMF-28e fiber with GVD of −21 $ps^2 \cdot km^{-1}$ at 1.5μm into the ring cavity, which was considered as a simple and effective approach to optimize the net cavity dispersion to be anomalous.

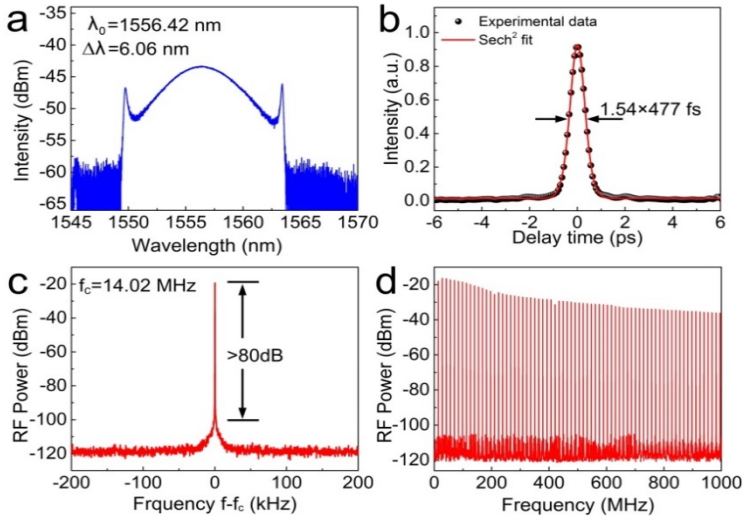

Fig. 5. Mode-locking characteristics of the 1.5 μm EDF laser. (a) Output optical spectrum with solitonic sidebands. (b) AC trace of mode-locked pulse with a $sech^2$ fitting curve. (c) The fundamental frequency of typical RF spectrum of the output mode-locked pulse train. (d) The wideband RF spectrum in the 1GHz span.

The self-starting mode-locking operation was realized in the EDF laser cavity with a total cavity length of ~14 m, when the pump power reached the threshold of 160 mW. Figure 5(a) shows the optical spectrum of the mode-locked pulses with central wavelength of 1556.42 nm and a bandwidth of 6.06 nm. The Kelly sidebands are symmetrically distributed at two sides

of spectrum, attributed to the periodic soliton perturbation in the laser cavity, verified that the mode-locked laser operates at the soliton state. The autocorrelation (AC) trace of the mode-locked pulses is shown in Fig. 5(b), well fitted by a $sech^2$ profile with 734.6 fs full width at half maximum (FWHM). After multiplying the AC trace width with the de-correlation factor of 0.648 for the $sech^2$ pulses, the pulse duration is calculated to be 477 fs, which is the shortest for WSe_2 mode-locked fiber lasers [24]. From the measured 6.06 nm spectral bandwidth, the transform limit is calculated around 420 fs, which indicates the output pulses were slightly chirped. Figure 5(c) shows the radio-frequency (RF) spectrum of the mode-locked pulses at a fundamental repetition rate of 14.02 MHz. The signal-to-noise ratio (SNR) is larger than 80 dB (10^8 contrast), which is much better than that of the previously reported mode-locked fiber laser based on WSe_2 nanosheets [24]. The wideband RF spectrum recorded within a 1 GHz span is presented in Fig. 5(d), which indicates the good stability of the mode-locked pulses. Self-starting mode-locking was also achieved with different cavity lengths. As we increase the cavity length up to 80 m, the pulse duration was in this case 1.23 ps. Worth noting that shorter pulse width can be realized by further optimizing the cavity length with approximate zero dispersion in cavity [39].

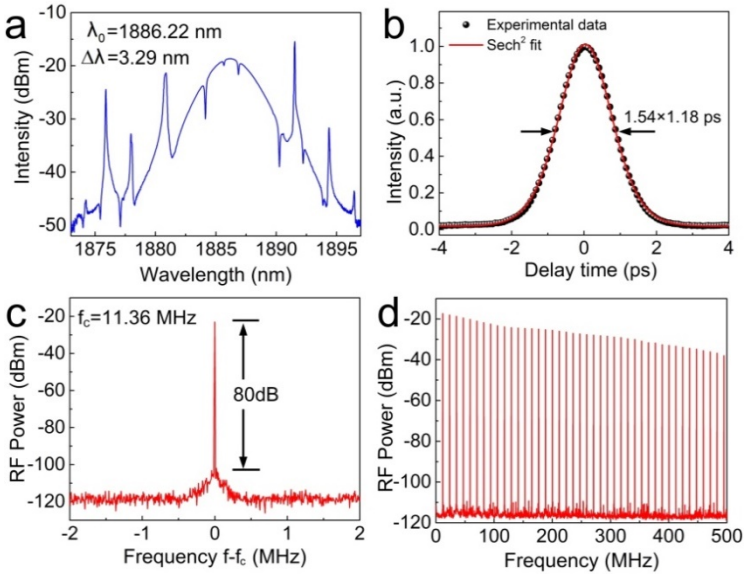

Fig. 6. Mode-locking pulse output characterizations of the 1.9 μm TDF laser. (a) Optical spectrum of the soliton mode-locked pulse overlapped with water absorption lines. (b) The AC trance with 1.18 ps pulse duration. (c) The fundamental frequency of 11.36 MHz. (d) The wideband RF spectrum.

Recent demonstrations indicated that several kind of 2D materials, like graphene [33], black phosphorus [34], WS_2 [35], and $MoSe_2$ [36], show broadband nonlinear optical absorption, which have been used as SA for mode-locking operation. However, thus far, mode-locked laser at 2 μm region based on WSe_2 has not been fully investigated. Here, we demonstrated the WSe_2 mode-locked fiber laser at this region. The 2 μm mode-locked laser cavity was shown in Fig. 4(d). A piece of 2.3 m TDF with -20 $ps^2 \cdot km^{-1}$ dispersion at 2.0 μm was used as the gain medium, which was reversely pumped by a 1550 nm LD through a 1550/2000 nm WDM. Other fiber components, including PI-ISO, PC, OC (20/80), work at 1.9 μm. The connect fiber between each components was SMF-28e fiber with -71 $ps^2 \cdot km^{-1}$ dispersion at 2.0 μm. The total cavity length of TDF laser cavity was around 18 m. The output optical spectrum was recorded by an optical spectrum analyzer (Yokogawa AQ6375B). Stable mode-locking operation was realized after the pump power exceeds the threshold value

Optics EXPRESS

of 650 mW. We believe that the high mode-locking threshold mainly results from the bending loss of the SMF-28e fiber and large transmission loss (~90%) of the microfiber at 2 μm region. As the pump power increased up to 1310 mW, the laser remained in the mode-locked state with 32.5 mW output power. The high output power reveals that the microfiber WSe_2 SA possesses high thermal damage threshold (0.137 $GW \cdot cm^{-2}$). The mode-locking performance was characterized at the maximum pump power of 1310 mW. Figure 6(a) shows the output optical spectrum with 1886.22 nm central wavelength and 3.29 nm FWHM bandwidth. The Kelly sidebands on optical spectrum confirm the soliton mode-locked state in the anomalous dispersion regime. The dips on optical spectrum are probably originated from strong water absorption lines located in the 1.9 μm region [34]. The AC trace of the mode-locked pulses with a $sech^2$ fitting is depicted in Fig. 6(b). The pulse duration is 1.18 ps after deconvolution. The RF spectrum of mode-locked pulses is shown in Fig. 6(c). The repetition rate is equal to 11.36 MHz matching well with the cavity roundtrip time (18 m cavity length), and the SNR is larger than 80 dB, comparable to that of our mode-locked 1.55 μm laser based on WSe_2. The RF spectrum in the 500 MHz span confirms the stability and uniformity of the output pulse train. In addition, we measured the PDL within a small range of 9.52%~9.71% at 1990 nm with 5.84 mW input power, which confirms that the undesired NPE effect could be avoided at 1.9 μm region in this cavity.

Table 1. Comparison of mode-locked lasers based on different 2D materials[a]

Materials	Fabrication	Integration	τ	λ/FWHM	α_s	SNR	Ref.
Graphene	CVD	Fiber end face	756	1565/5	6.2-66.5	65	40
	LPE	Fiber end face	464	1559/5.24	~1.3	84	41
	CVD	Mirror	729	2018/7.3	~1	-	33
Black Phosphorus	ME	Fiber end face	739	1910/5.8	10.6	>70	34
	ME	Fiber end face	786	1558.7/6.2	-	56	43
MoS_2	CVD	Fiber end face	1268	1568.9/2.6	35.4	~62	26
WS_2	CVD	Fiber end face	1490	1568.3/1.94	15.1	71.8	14
WSe_2	LPE	Side-polished fiber	1310	1556.7/2	0.3	-	24
		Fiber end face	1250	1557.6/2.1	0.5	-	
	CVD	Microfiber	477	1556.4/6.06	54.5	>80	This work
			1180	1886.2/3.29	~1.83	80	

[a]CVD, chemical vapor deposition; LPE, liquid phase exfoliation; ME, mechanical exfoliation; τ, pulse duration (fs); λ/FWHM, central wavelength (nm)/ full width at half maximum (nm); α_s, modulation depth (%); SNR, signal-to-noise ratio (dB).

As we remove the microfiber WSe_2 SA from laser cavity, no mode-locked pulses can be observed in both EDF and TDF laser systems, no matter how we increase the pump power or turn the angle of the PC in a wide range. This verifies that the microfiber WSe_2 SA plays a critical role in mode-locking operation. The performance comparison of mode-locked lasers based on different 2D materials is listed in Table 1. The mode-locked operations are realized at both 1.5 and 2.0 μm, and the ultrashort pulse duration is achieved up to hundreds of femtosecond. Compared to the extensively studied 2D materials SA such as graphene, black phosphorus, MoS_2, and WS_2 [33–38,40–45], large-area WSe_2 has less been reported in ultrashort pulse generation. This contribution provides the compelling evidence of WSe_2 as excellent SAs for ultrafast photonic applications. Moreover, the optical properties and photonic applications of WSe_2 have not yet been fully explored up to now. For example, the promising WSe_2 p-n junction and heterojunction contacted with other 2D materials possessing unique energy band structure and charge transport characteristics have attracted much interest in electronic and optoelectronic devices [21,22], while their potential applications in ultrafast photonic are worth to be further investigated.

Optics EXPRESS

5. Summary

Summarily, we have demonstrated CVD-grown large-area WSe_2 films as SAs for passively mode-locked fiber lasers at 1.5 and 2 μm region. The CVD growth process was presented in details, and material characterizations indicated the high quality of the as-grown large-area WSe_2 film. By employing a PMMA assisted transfer method, the large-area WSe_2 film was successfully transferred onto the side wall of a microfiber to fabricate a WSe_2 SA with enhanced light-WSe_2 interaction through the strong evanescent wave coupling effect. As a result, the WSe_2 SA shown an extraordinarily large modulation depth of 54.5%. For the EDF laser system, highly stable mode-locked pulses were obtained with the pulse duration of 477 fs. The stable mode-locking operation at both 1.5 and 2 μm regions suggests that the large-area WSe_2 film was an excellent broadband SA for ultrafast photonics.

Funding

National Natural Science Foundation of China (NSFC) (61775146, 61575129, 51502176, 61605122); China Postdoctoral Science Foundation (2015M582408); Natural Science Foundation of Guangdong Province (2016A030310059, 2016A030310049); Shenzhen Science and Technology Project (JCYJ20160422103744090, JCYJ20170302142929402, JCY20150324141711695, JCYJ20160427105041864, KQJSCX20160226194031, JCYJ20150324141711618, JSGG20160429114438287).